IEEE Access
Multidisciplinary | Rapid Review | Open Access Journal

Received 15 July 2024, accepted 6 August 2024, date of publication 12 August 2024, date of current version 20 August 2024.

Digital Object Identifier 10.1109/ACCESS.2024.3441929

RESEARCH ARTICLE

Toward Humanlike Passive Dynamic Walking With Physical and Dynamic Gait Resemblance

MAHAN JABERI MIANDOAB[1], MOHAMMAD REZA HAGHJOO[2], AND BORHAN BEIGZADEH[1]

[1]Biomechatronics and Cognitive Engineering Research Laboratory, School of Mechanical Engineering, Iran University of Science and Technology, Tehran 16846-13114, Iran
[2]Department of Mechanical and Energy Engineering, Shahid Beheshti University, Tehran 1983969411, Iran

Corresponding author: Borhan Beigzadeh (b_beigzadeh@iust.ac.ir)

ABSTRACT In this study, we present the first passive walking model on a slope to have exact anthropomorphic physical parameters in addition to the ability to closely reproduce the dynamic gait of humans. To simulate the stance phase, we utilized knee joints with variable stiffness instead of the locking mechanism that is prevalent among passive models with knees. Additionally, the model has flat feet with ankle compliance to include the distinctive double stance phase of human walking in the gait pattern. The stiffness and damping parameters of the joints are then adjusted to increase the resemblance between the model and gait data of human walking reported in literature. Following the comparison between the joint trajectories of the model and humans, it is demonstrated that the presented model displays a gait that is substantially more comparable with human walking than previous attempts at modeling humanlike passive walkers. The resulting model shows great potential, as semi-passive and efficient active walkers can be developed based on its natural humanlike dynamics. Furthermore, it may be possible to utilize this walker to simulate the complex behaviors of the human gait under different conditions and facilitate the design stages of rehabilitative or assistive devices by decreasing the need for expensive human trials and experiments.

INDEX TERMS Biomimetics, humanoid and bipedal locomotion, legged robots, passive walking.

I. INTRODUCTION

The human gait presents one of the most complex forms of movement as we are able to maintain a dynamically stable gait and modify it according to the terrain we walk on. There are many conditions, however, that may adversely affect our ability to walk with ease. Consequently, it is essential to develop different rehabilitative devices or prosthetic limbs to help patients with lower-limb mobility impairment. Although human trials are unavoidable in this process, predictive multibody models [1] can be utilized in simulations to facilitate the earlier stages of design. Predictive musculoskeletal models vary in complexity [2] and need to be optimized to reduce their high computational cost [3]. However, skeletal models such as bipedal robots [4] can result in simulations that are computationally more efficient and provide acceptable results [5], [6]. Many humanlike bipedal robots have been designed with the goal of studying the characteristics of human gait. While these motorized robots have the ability to walk and run [7], the gait produced by their precise joint-angle control method either looks unnatural or requires significant amounts of energy which results in inefficient locomotion [8]. As a result, these types of robots and the employed control approach, are not suitable to be a platform for studying an architectural design of assistive and rehabilitative devices such as wearable robots, actuated orthoses, and prostheses. Meanwhile, there is a group of unactuated walkers that can maintain a dynamically stable gait down a slope while their movement solely depends on their mechanical properties and the terrain they walk on. These walkers, better known as passive dynamic walkers, were first introduced by McGeer [9] and their dynamic behavior can be explained by studying the motion of a rimless wheel [10]. Interestingly, these robots have gait patterns similar to the human gait

The associate editor coordinating the review of this manuscript and approving it for publication was Jingang Jiang.

which could stem from the fact that while humans do not walk passively, their locomotion is minimally actuated. It is demonstrated in [11] that a simple passive walker can achieve stable walking on level ground with the help of an impulsive actuator that is applied to the trailing foot just before the heel strike. Additionally, this impulse which approximates the muscle activity in the human leg before toe-off, results in a gait that is more efficient than applying torque on the stance leg. Choi et al. [12] also used this impulsive actuator in a 5-link model during the double stance phase to study the possibility of more efficient walking robots. Based on these studies, the steady, efficient, and humanlike gaits that can be obtained with minimal actuation and the utilization of the natural dynamics of the systems may suggest that the human gait can be closely simulated with passive dynamic walkers.

Passive dynamic walkers often have simpler designs compared to their active counterparts as the simplest passive biped [13] comprises only two links called the stance and swing leg. This model, also called the compass-like walker [14], can be used to study various aspects of passive dynamic walking such as the basin of attraction of stable gaits [15] and the effects of a switching surface on stability [16]. Moreover, this model can be modified to develop more complicated walkers by including an upper body, knees, and feet in the model. The upper body link can be implemented by using a kinematic coupling [17] or torsional springs [18] in the hip joints. Furthermore, the addition of knees [19] can prevent the foot scuffing that occurs in knee-less models while the inclusion of feet can significantly affect the characteristics of the resulting motion. The effect of passive feet on the gait can be studied by adding ankle stiffness [20] or modeling different types of feet. Knee-less [21] and kneed models [22] with flat feet have been developed that can include the double-stance phase which is a distinctive part of human locomotion. Moreover, walkers with flat feet are able to generate various stable gait patterns [23] where the model follows different phases depending on the parameters of the system. In a recent study [24], a passive walker is modeled with feet that mimic the human rollover shape and a viscoelastic kneecap that prevents hyperextension but lacks the ankle compliance and variable gait patterns that are present in walkers with flat feet. Another study [25] shows that stiff stance legs do not accurately simulate the walking dynamics of the human stance leg by modeling a walker with two massless linear springs as legs and a point mass at the hip. Planar passive models can be transformed into three-dimensional walkers [26] which will include lateral stability. Studying passive dynamics in three-dimensions, in addition, allows the concept of passive turning to be studied in a rimless wheel [27] and bipeds [28]. The characteristics of passive bipeds are further studied by building two-dimensional [29] and three-dimensional [30] walkers based on the principals of passive dynamics that can provide valuable information about the effects of structural changes on the resulting gaits. For example, one study [31] focuses on the ankle and toe functions and their role in the overall walking stability by developing a three-dimensional passive walker while the study in [32] discusses swing leg control for fall prevention.

The dynamic stability of passive walkers can be utilized to design passivity-based controlled robots [33] which can exploit the natural dynamics of the system to walk with noticeably lower energy costs than walkers with trajectory-tracking control methods. Other methods can be used to control passive walkers such as the OGY-based controller in [34] and [35] and the adaptive speed controller in [36]. In addition, passive manipulators [37] can be designed which follow the principles of passive dynamics as shown in [38] where passive walking is defined as a special case of passive manipulation.

The similarity between the gait of dynamically stable passive models and human locomotion has resulted in several studies utilizing them in designing neuromuscular models of the human legs [39] and lower-limb prostheses. For example, the kneed model in [40] with asymmetric parameters was utilized to design a prosthesis for patients with unilateral lower-limb amputation [41]. While this model includes asymmetry by having different physical parameters for each leg, an underactuated model was studied in [42] where the asymmetric behavior stemmed from one leg of the model being knee-less. Based on this walker, a fully passive three-link asymmetric walker is studied in [43] where the possibility of obtaining a gait with symmetric step lengths and its benefits are discussed. A passive exoskeleton is designed in [44] by simulating a ballistic walker to study the energy consumption of the system. Moreover, some movement disorders such as Parkinson's disease can be studied by simulating chaotic models of passive dynamic walking [45]. While simple passive walkers cannot compete with the accuracy of musculoskeletal models available in software such as OpenSim [46], a recent study, which discussed the suitability of different gait models for the simulation of walking with body weight support [47], demonstrated that the simpler spring-loaded inverted pendulum model in [25] can present better results than a neuromuscular model [39] in some cases.

Although passive walkers can have many applications, there seems to be a shortcoming in the development of passive bipeds that can include the main characteristics of the human locomotion in their gait in addition to having anthropomorphic parameters. This could be due to the challenges of simulating stable passive walkers as smallest changes in the parameters can lead to unstable gaits or result in walking patterns that are not similar to human locomotion. Moreover, simulating a passive walker with exact humanlike parameters becomes significantly more challenging as the number of variables that can be changed to make the gait stable becomes very limited. As a result, apart from one study which models a passive walker with point feet and humanlike

TABLE 1. The parameters of the model.

Parameter	Description	Value
l_s	Shank length	0.388 m
l_t	Thigh length	0.379 m
l_f	Foot length	0.15 m
l_{sc}	Shank COM (from ankle to COM)	0.2312 m
l_{tc}	Thigh COM (from knee to COM)	0.2361 m
l_{fc}	Foot COM (from ankle to COM)	0.0273 m
l_{ft}	Distance from toe to ankle	0.12 m
l_{fh}	Distance from heel to ankle	0.03 m
m_h	Hip mass	35.88 kg
m_t	Thigh mass	8.76 kg
m_s	Shank mass	2.7 kg
m_f	Foot mass	0.6 kg
J_t	Mass moment of inertia of thigh	0.1288 kg.m^2
J_s	Mass moment of inertia of shank	0.0319 kg.m^2
J_f	Mass moment of inertia of foot	0.0009 kg.m^2

mass proportions [48], there are not any direct comparisons between kneed passive walkers and humans.

In this paper, we present a planar passive walker with exact humanlike parameters that consists of legs that can display a dynamic behavior similar to humans. While a conventional passive walker with simple knees can simulate the behavior of the swing leg, it lacks the weight acceptance phase which is an essential part of human locomotion. This is due to the locking mechanism that is responsible for keeping the stance leg straight. To resolve this, we discuss the possibility of adding a variable stiffness mechanism to the knees by using torsional springs that are engaged during a portion of the stance phase. Additionally, we utilize flat feet and ankle compliance in the model which provides a double stance phase for a more humanlike motion.

II. METHODS

A. THE HUMANLIKE PASSIVE MODEL

The walker presented here has anthropomorphic parameters, meaning that the mass, inertial parameters, and the length of each link are similar to the corresponding limb of the human leg. These parameters are extracted from the Handbook of Human Motion [49] for an average 60kg female as listed in Table 1. The model consists of six links which are two flat feet, two shanks and two thighs as depicted in Fig. 1, where q_1, q_2, q_3, q_4, q_{f1}, and q_{f2} indicate the absolute angle of the stance leg shank, the stance leg thigh, the swing leg thigh, the swing leg shank, the stance foot, and the swing foot respectively. Since we do not include an upper body in this model, we assume that the upper body mass is concentrated on the hip.

A series of torsional springs and dampers are needed for the walker to maintain stability. The damping and stiffness values in the ankles of both legs are assumed to be constant throughout the gait. In passive bipeds which include a knee joint, the stance leg is assumed to be kept straight with a locked knee. This requires the full extension of the leg with an

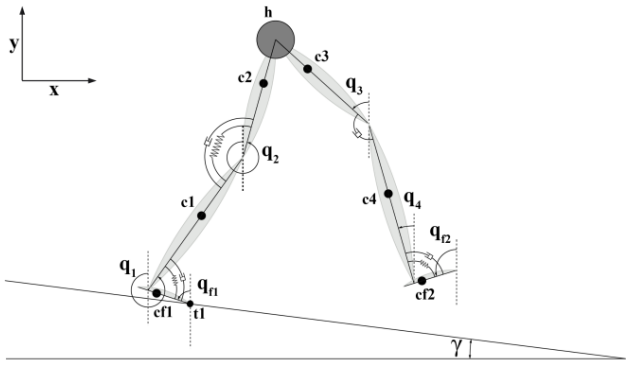

FIGURE 1. The schematic of the 6-link humanlike biped presented in this paper.

impact called the knee strike during the prior swing phase to maintain balance. Unlike these models, the human knee is not locked in the stance phase and instead, acts like a spring with high stiffness. This characteristic is explored in [25]. To replicate this behavior in a model with articulated legs, we assume that torsional springs are present in the knee joints which are engaged during a portion of the stance phase. Additionally, this removes the need for the swing knee strike to occur as the locked-swing-leg phase which is present in kneed passive walkers is no longer witnessed. The moment at which this spring is engaged or disengaged will be discussed in later paragraphs. The damper in the swing knee is assumed to have different values whether the knee is flexing or extending. This value is set to be higher during knee extension to prevent hyperextension in the swing knee. When the stiff torsional spring is engaged in the stance knee, we assume that the damping values during flexion and extension become equal to the higher damping value in the swing knee.

B. WALKING DYNAMICS

The walker's configuration can be described by rectangular coordinates $\boldsymbol{r}$ which comprises the mass center position of each link along the x- and y-axis and their absolute angles as:

$$\boldsymbol{r} = [x_{c1}; y_{c1}; q_1; x_{c2}; y_{c2}; q_2; x_{c3}; y_{c3}; q_3; x_{c4}; y_{c4}; q_4; x_h; y_h; x_{cf1}; y_{cf1}; q_{f1}; x_{cf2}; y_{cf2}; q_{f2}]. \quad (1)$$

Additionally, the generalized coordinates vector $\boldsymbol{q}$ which comprises the absolute angles of each link and the position of the stance toe is described as:

$$\boldsymbol{q} = \left[q_1; q_2; q_3; q_4; q_{f1}; q_{f2}; x_{t1}; y_{t1}\right]. \quad (2)$$

The position of the stance toe, which is the leading leg at the beginning of each step, is added to the generalized coordinates to obtain the ground reaction forces throughout the gait. Matrix T transfers generalized velocities $\dot{\boldsymbol{q}}$ into velocities in rectangular coordinates $\dot{\boldsymbol{r}}$ and it is defined as follows:

$$T = \frac{d\boldsymbol{r}}{d\boldsymbol{q}}. \quad (3)$$

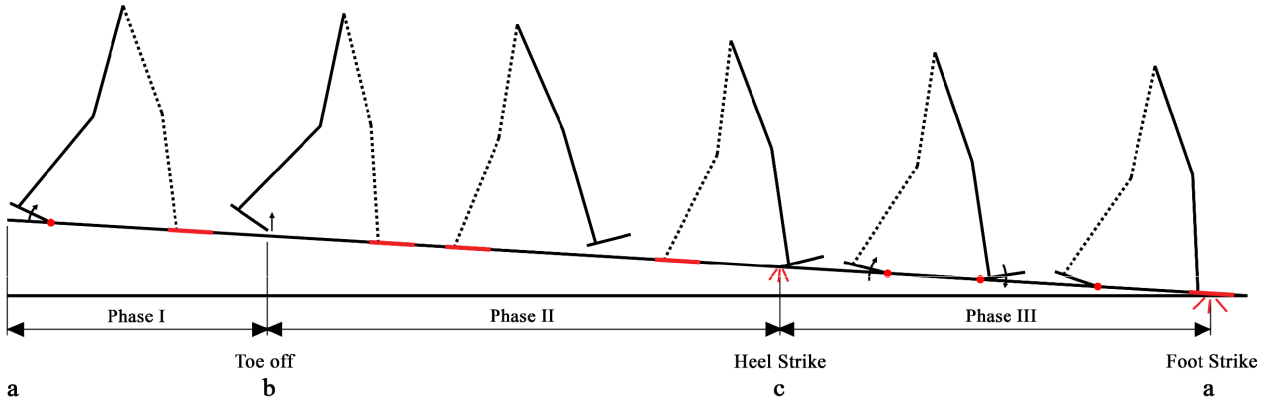

FIGURE 2. The walking phases of the humanlike passive walker.

A set of constraints are required to define the properties of each phase which are described by the constraint function as:

$$\boldsymbol{\varepsilon}(\boldsymbol{q}) = 0. \tag{4}$$

Equation (4) can be transformed into the following equation:

$$\boldsymbol{E}\ddot{\boldsymbol{q}} + \frac{\partial(\boldsymbol{E}\dot{\boldsymbol{q}})}{\partial \boldsymbol{q}}\dot{\boldsymbol{q}} = 0, \tag{5}$$

where

$$\boldsymbol{E} = \frac{\partial \boldsymbol{\varepsilon}(\boldsymbol{q})}{\partial \boldsymbol{q}}. \tag{6}$$

The equation of motion is obtained by utilizing Lagrange's equation of first kind:

$$\boldsymbol{M}_q\ddot{\boldsymbol{q}} = \boldsymbol{F}_q + \boldsymbol{E}^T\boldsymbol{\lambda}, \tag{7}$$

where $\boldsymbol{M}_q$ is the generalized mass matrix, $\boldsymbol{F}_q$ is the generalized forces and λ is the vector of constraint forces required to enforce each constraint in (4). $\boldsymbol{M}_q$ and $\boldsymbol{F}_q$ are obtained from $\boldsymbol{M}$ and $\boldsymbol{F}$ as:

$$\boldsymbol{M}_q = \boldsymbol{T}^T\boldsymbol{M}\boldsymbol{T}, \tag{8}$$

and

$$\boldsymbol{F}_q = \boldsymbol{T}^T\boldsymbol{F} - \boldsymbol{T}^T\boldsymbol{M}\frac{\partial \boldsymbol{T}}{\partial \boldsymbol{q}}\dot{\boldsymbol{q}}\dot{\boldsymbol{q}}, \tag{9}$$

where

$$\begin{aligned}\boldsymbol{M} = [&m_s; m_s; J_s; m_t; m_t; J_t; m_t; m_t; J_t; m_s; m_s; J_s; m_h; m_h;\\ &m_f; m_f; J_f; m_f; m_f; J_f],\end{aligned} \tag{10}$$

and

$$\begin{aligned}\boldsymbol{F} = [&0; -m_s g; T_1; 0; -m_t g; T_2; 0; -m_t g; T_3; 0; -m_s g; T_4;\\ &0; -m_h g; 0; -m_f g; T_{f1}; 0; -m_f g; T_{f2}].\end{aligned} \tag{11}$$

In (11), T_1, T_2, T_3, T_4, T_{f1}, and T_{f2} refer to the torques acting on the stance shank, stance thigh, swing thigh, swing shank, stance foot, and the swing foot respectively and g is gravitational acceleration. By combining (5) and (7) we have the constrained equation of motion as:

$$\begin{bmatrix}\boldsymbol{M}_q & -\boldsymbol{E}^T\\ \boldsymbol{E} & 0\end{bmatrix}\begin{bmatrix}\ddot{\boldsymbol{q}}\\ \boldsymbol{\lambda}\end{bmatrix} = \begin{bmatrix}\boldsymbol{F}_q\\ -\frac{\partial(\boldsymbol{E}\dot{\boldsymbol{q}})}{\partial \boldsymbol{q}}\dot{\boldsymbol{q}}\end{bmatrix}. \tag{12}$$

C. PHASES AND IMPACTS

Each successful step consists of three phases with three events defining the end of each phase as depicted in Fig. 2. There are two impacts in each step (i.e., the heel strike (**c**) and the foot strike (**a**)) which are assumed to be instantaneous and fully inelastic. This assumption allows the use of the principle of conservation of angular momentum to obtain the post-impact state vectors of the system.

The first phase (phase I) begins instantly after the foot strike of the leading leg. This instant is chosen as the initial state to reduce the number of parameters needed to simulate the gait as the angular velocity of the leading foot ($\dot{q}_{f1}$) is equal to zero and its absolute angle is known following the foot-strike ($q_{f1} = \pi/2 - \gamma$). In this phase, the leading foot keeps full contact with the ground while the trailing foot rotates about its toe until it loses contact with the ground. The constraint function for this phase is:

$$\varepsilon_A = \begin{bmatrix} x_{cf2} + (l_{ft} - l_{fc})\sin q_{f2}\\ y_{cf2} - (l_{ft} - l_{fc})\cos q_{f2}\\ x_{t1}\\ y_{t1}\\ l_f\cos(q_{f1}) - y_{h1}\end{bmatrix}, \tag{13}$$

where x_{cf2} and y_{cf2} are the position of the mass center of the trailing foot along the x and y axis respectively. The first two constraints are to keep the trailing toe in contact with the ground while the last three constraints force the leading foot to keep full contact with the ground. y_{h1} in the last constraint is a constant value which is equal to the position of the leading heel along the y axis. Phase I ends when the toe of the trailing foot loses contact with the ground. This event is detected when the reaction force which is perpendicular to the ground at the trailing toe becomes negative. There are no impacts at

the end of this phase, therefore, the state vector required to simulate the next phase is readily available.

Phase II, which begins after the toe off (**b**), accounts for the longest phase as the swing leg swings forward while the stance foot maintains full contact with the ground. Since only three constraints are needed to keep the stance foot in full contact with the ground, the constraint function for this phase can be obtained as:

$$\varepsilon_B = \begin{bmatrix} x_{t1} \\ y_{t1} \\ l_f \cos\left(q_{f1}\right) - y_{h1} \end{bmatrix}. \tag{14}$$

The end of this phase is detected when the heel of the swing foot has an impact with the ground. Since the impact is instantaneous, the absolute angles of the links are kept constant. As a result, we only need to find the post-impact velocities to simulate the next phase. There are impulses under both feet at the moment of impact. We assume that the trailing heel rises just after the impact, so the corresponding impulse of this foot is located at the toe. Moreover, the impulse at the leading heel is excluded from the equations as the walker's angular momentum is calculated with respect to this point. Eight post-impact values need to be calculated which include the angular velocities of every link and the horizontal and vertical components of the impulse at the trailing toe. Six equations are obtained by utilizing the principle of conservation of angular momentum as follows:

- Conservation of the angular momentum of the whole walker about the leading heel.
- Conservation of the angular momentum of the trailing leg, the hip, the leading thigh, and the leading shank about the leading ankle.
- Conservation of the angular momentum of the trailing leg, the hip, and the leading thigh about the leading knee.
- Conservation of the angular momentum of the trailing leg about the hip.
- Conservation of the angular momentum of the trailing foot and the trailing shank about the trailing knee.
- Conservation of the angular momentum of the trailing foot about the trailing ankle.

The two remaining equations are obtained by calculating the horizontal and vertical velocity components of the hip about the trailing toe and the leading heel. The corresponding velocity components have to be equal in order to satisfy the constraints in the next phase. These equations are then obtained as:

$$\begin{cases} \boldsymbol{L}^+_{Fh2} = \boldsymbol{L}^-_{Fh2} + (\boldsymbol{P}_{Ft1} - \boldsymbol{P}_{Fh2}) \wedge \boldsymbol{I} \\ \boldsymbol{L}^+_{A2} = \boldsymbol{L}^-_{A2} + (\boldsymbol{P}_{Ft1} - \boldsymbol{P}_{A2}) \wedge \boldsymbol{I} \\ \boldsymbol{L}^+_{K2} = \boldsymbol{L}^-_{K2} + (\boldsymbol{P}_{Ft1} - \boldsymbol{P}_{K2}) \wedge \boldsymbol{I} \\ \boldsymbol{L}^+_{H} = \boldsymbol{L}^-_{H} + (\boldsymbol{P}_{Ft1} - \boldsymbol{P}_{H}) \wedge \boldsymbol{I} \\ \boldsymbol{L}^+_{K1} = \boldsymbol{L}^-_{K1} + (\boldsymbol{P}_{Ft1} - \boldsymbol{P}_{K1}) \wedge \boldsymbol{I} \\ \boldsymbol{L}^+_{A1} = \boldsymbol{L}^-_{A1} + (\boldsymbol{P}_{Ft1} - \boldsymbol{P}_{A1}) \wedge \boldsymbol{I} \\ \dot{x}^+_{HFt1} = \dot{x}^+_{HFh2} \\ \dot{y}^+_{HFt1} = \dot{y}^+_{HFh2}, \end{cases} \tag{15}$$

where $\boldsymbol{I}$ is the impulse vector at the trailing toe and $\boldsymbol{L}$ is the angular momentum about the point indicated by the subscript. Moreover, $\boldsymbol{P}$ is the position of the point indicated by the subscript. The subscripts $Ft1$, $A1$, $K1$, H, $K2$, $A2$, and $Fh2$ indicate the trailing toe, the trailing ankle, the trailing knee, the hip, the leading knee, the leading ankle, and the leading heel respectively. The superscripts $+$ and $-$ denote the post-impact and the pre-impact variables respectively. After the post-impact variables are obtained, it is important to monitor the value of impulse at the trailing toe perpendicular to the ground. This value needs to be positive to satisfy the initial assumption, otherwise, another gait pattern will be followed in which the trailing heel remains in contact with the ground, or the foot rises completely. Since the desired gait includes the heel-rise at the moment of impact, the parameters are chosen in a way to include this characteristic.

Immediately after the trailing heel loses contact with the ground, phase III begins in which the trailing foot rotates about its toe while the leading foot rotates about its heel. These contacts are enforced by the following constraint equation as:

$$\varepsilon_C = \begin{bmatrix} x_{t1} \\ y_{t1} \\ x_{cf2} - \left(l_{fh} + l_{fc}\right) \sin q_{f2} \\ y_{cf2} + \left(l_{fh} + l_{fc}\right) \cos q_{f2} \end{bmatrix}. \tag{16}$$

This phase continues until the leading foot rotates to have an impact to be in full contact with the ground (**a**).

Unlike the heel strike in which the positions of both impulses are known based on the assumptions, the position of the impulse under the leading foot is unknown during the foot strike. Therefore, one more equation is needed compared to the heel strike which is obtained with the assumption that the leading foot keeps full contact with the ground after impact. The principle of conservation of angular momentum is utilized as follows:

- Conservation of the angular momentum of the whole walker about the trailing toe.
- Conservation of the angular momentum of the leading leg, the hip, the trailing thigh, and the trailing shank about the trailing ankle.
- Conservation of the angular momentum of the leading leg, the hip and the trailing thigh about the trailing knee.
- Conservation of the angular momentum of the leading leg about the hip.
- Conservation of the angular momentum of the leading foot and the leading shank about the leading knee.
- Conservation of the angular momentum of the leading foot about the leading ankle.

Moreover, the velocity of the hip with respect to the leading ankle and the trailing toe needs to be equal post-impact to enforce the constraints of the next phase. The required

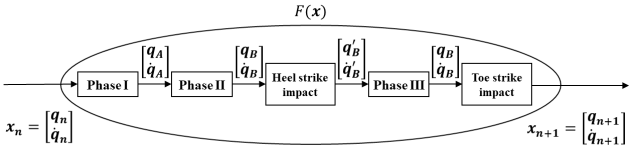

FIGURE 3. Function mapping the initial state vector of the nth step to the state vector of the (n+1)th step.

equations are then:

$$\begin{cases} \boldsymbol{L}_{Ft1}^{+} = \boldsymbol{L}_{Ft1}^{-} + (\boldsymbol{P}_{A2} + \boldsymbol{R} - \boldsymbol{P}_{Ft1}) \wedge \boldsymbol{I} \\ \boldsymbol{L}_{A1}^{+} = \boldsymbol{L}_{A1}^{-} + (\boldsymbol{P}_{A2} + \boldsymbol{R} - \boldsymbol{P}_{A1}) \wedge \boldsymbol{I} \\ \boldsymbol{L}_{K1}^{+} = \boldsymbol{L}_{K1}^{-} + (\boldsymbol{P}_{A2} + \boldsymbol{R} - \boldsymbol{P}_{K1}) \wedge \boldsymbol{I} \\ \boldsymbol{L}_{H}^{+} = \boldsymbol{L}_{H}^{-} + (\boldsymbol{P}_{A2} + \boldsymbol{R} - \boldsymbol{P}_{H}) \wedge \boldsymbol{I} \\ \boldsymbol{L}_{K2}^{+} = \boldsymbol{L}_{K2}^{-} + (\boldsymbol{P}_{A2} + \boldsymbol{R} - \boldsymbol{P}_{K2}) \wedge \boldsymbol{I} \\ \boldsymbol{L}_{A2}^{+} = \boldsymbol{L}_{A2}^{-} + (\boldsymbol{R}) \wedge \boldsymbol{I} \\ \dot{x}_{HFt1}^{+} = \dot{x}_{HA2}^{+} \\ \dot{y}_{HFt1}^{+} = \dot{y}_{HA2}^{+} \\ \dot{q}_{f2}^{+} = 0, \end{cases} \tag{17}$$

where the vector $\boldsymbol{R}$ indicates the distance from the leading ankle to the position of impulse under the leading foot. The roles of the legs are switched after this phase to begin the simulation of the next step. The values of the reaction forces are continuously checked during the simulations to ensure that the resulting gaits follow the desired walking pattern.

D. STABLE GAIT DETECTION

To find a stable gait, we use the method of Poincare' mapping [50] and simulate the model by solving the equations of motion numerically with the ODE45 function in MATLAB which is based on an explicit Runge-Kutta (4,5) formula [51]. We choose the start of each step as our Poincare' section and try to find the fixed point for each step's Poincare' map. The gait is stable if the resulting limit cycle is asymptotically stable. This means that for small perturbations in the initial state vector, the following state vectors at the beginning of each step get closer to the fixed point. Consider $F(x_n)$ as the Poincare' mapping function (Fig. 3) which maps the nth initial state vector to the (n+1)th initial state vector as:

$$x_{n+1} = F(x_n). \tag{18}$$

The fixed point of this mapping can be found by changing the compliance parameters of the model to minimize the function $G(x_n)$ for two consecutive steps which is described as:

$$G(x_n) = F(x_n) - x_n, \tag{19}$$

where $G(x_n) = 0$ means that the Poincare' function's output corresponds to the input and x_n is a fixed point for the system.

We used the Global Search function in MATLAB to minimize G. To study the stability of the fixed point, (18) is linearized for small perturbations δx as:

$$F(x^* + \delta x) \approx F(x^*) + J\delta x, \tag{20}$$

TABLE 2. The fixed point of a stable gait.

Symbol	Description	Value	Unit
q_1	Leading shank absolute angle	0.251697	rad
q_2	Leading thigh absolute angle	0.282955	rad
q_3	Trailing thigh absolute angle	-0.528919	rad
q_{f2}	Trailing foot absolute angle	1.415717	rad
$\dot{q}_1$	Leading shank angular velocity	-4.584169	rad/s
$\dot{q}_2$	Leading thigh angular velocity	2.053719	rad/s
$\dot{q}_3$	Trailing thigh angular velocity	1.704809	rad/s

TABLE 3. The compliance arrangement of the model.

Parameter	Value	Unit
Ankle stiffness	5.1045	N.m/rad
Ankle damping	0.8364	N.m.s/rad
Swing knee damping (flexion)	0.070	N.m.s/rad
Swing knee damping (extension)	1.199	N.m.s/rad
Stance knee stiffness	116.2	N.m/rad
Stance knee damping	1.199	N.m.s/rad
Knee spring equilibrium angle	0.0220	rad
Knee spring disengagement angle	0.0535	rad

where the Jacobian J is obtained as explained in [14]. If the state vectors of the steps subsequent to the perturbed initial state get closer to the fixed point, then the resulting gait is asymptotically stable. The eigen values of J, therefore, should be in the unit circle. Once a stable fixed point is found, it is possible to find other stable fixed points by changing the spring and damping coefficients at the joints. If the changes are small enough, the previous fixed point is likely to be in the basin of attraction of the new compliance arrangement. This is done to find a stable gait that resembles human locomotion as closely as possible.

III. RESULTS AND DISCUSSION

To ensure that both feet are in contact with the ground at the beginning of the first step as part of the constraints, the absolute angle of one link and the angular velocities of two links are obtained utilizing the constraint equations of phase I. We selected the angular velocity of the trailing foot ($\dot{q}_{f2}$) and the absolute angle and angular velocity of the trailing shank (q_4 and $\dot{q}_4$) as unknowns. Additionally, since the leading foot is in full contact with the ground, its absolute angle is known ($q_{f1} = \pi/2 - \gamma$), and its angular velocity ($\dot{q}_{f1}$) is equal to zero. We also assume that the leading toe is located on the origin of the x- and y-axis. Consequently, the initial state vector comprises seven values that are needed to simulate the gait. A stable fixed point for this model is obtained as listed in Table 2 at the beginning of phase I (Fig. 2) for a model with the joint stiffness and damping parameters in Table 3 and the slope angle of 0.1484 rad.

The corresponding limit cycles of the motion of one leg's shank and thigh during two consecutive steps are depicted

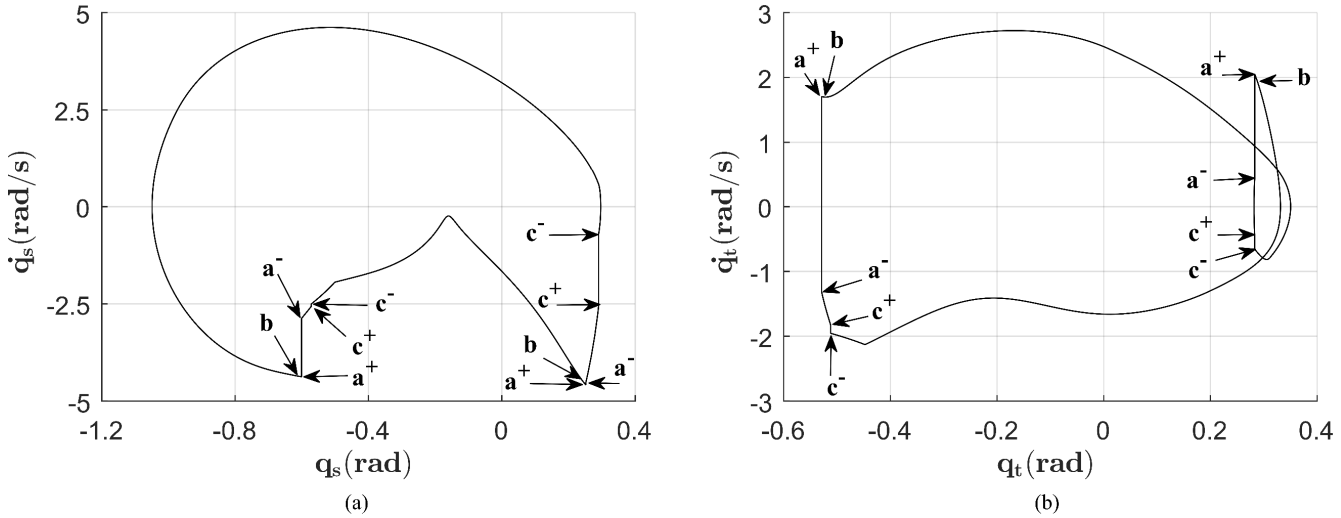

FIGURE 4. Limit cycle of the shank (a) and the thigh (b) of one leg in two consecutive steps.

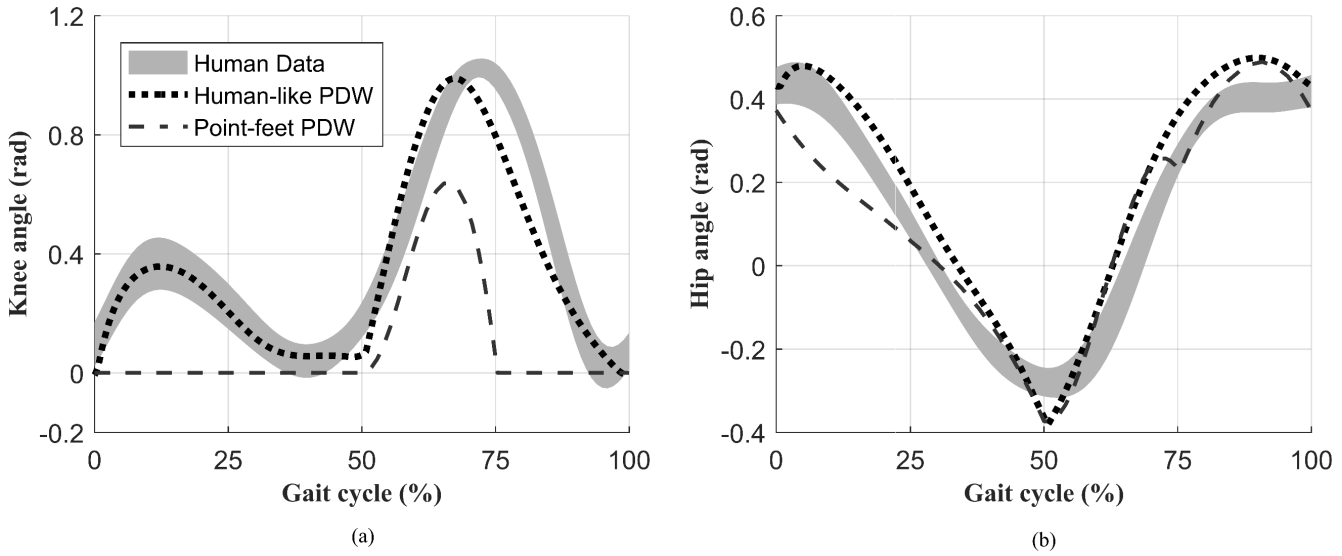

FIGURE 5. Comparison between the knee angle (a) and the hip angle (b) of the gait of the humanlike passive dynamic walker, human gait data and the PDW studied in [48].

in Fig.4 (a) and (b) respectively. The lower side of each limit cycle accounts for the stance phase while the upper portion corresponds to the swing phase of the gait. The points $\mathbf{a}^+$, $\mathbf{b}$, $\mathbf{c}^-$, $\mathbf{c}^+$, and $\mathbf{a}^-$ in Fig. 4 (a) and (b) indicate different key moments in the gait. Each step starts at point $\mathbf{a}^+$ which is the moment after the impact of the leading foot with the ground. The toe of the trailing leg loses contact with the ground at point $\mathbf{b}$ which is followed by the second phase of the gait. The heel strike occurs at $\mathbf{c}$ where the angular velocities of the shank and the thigh are changed from the values at $\mathbf{c}^-$ to $\mathbf{c}^+$ instantaneously. This impact affects the angular velocity of the leading shank more than the leading thigh. In contrast, the impact of the leading foot with the ground, which changes the state of the system from $\mathbf{a}^-$ to $\mathbf{a}^+$, has a bigger impact on the thigh than the shank. Due to the increase in the angular velocity of the leading thigh after the foot strike, the knee joint of the leading leg flexes to accept the weight of the model in the beginning of the next step.

The gait of the model can be compared with human locomotion by studying the similarities between the hip and knee angle of one leg during two consecutive steps and human gait data from [52]. Self-selected fast speed gait data for four female subjects with mass of 63.5kg, 65kg, 60.2kg, and 61.8kg and height of 1.60m, 1.69m, 1.66m, and 1.65m respectively were selected for comparison. The selection criteria included weight, height, and step length compatibility with the model and the obtained stable gait. The resulting diagrams, as depicted in Fig. 5 (a) for the knee and Fig. 5 (b)

for the hip angle respectively, begin from the heel-strike where the shaded area represents the standard deviation of the chosen human gaits. Since the human gait data is based on walking on a horizontal surface, the hip angle of the model is calculated relative to the ground for comparability. To compare human gait resemblance with previous attempts at modeling humanlike passive walkers, the walker studied in [48] is simulated and the knee and hip diagrams are depicted in Fig. 5 (a) and Fig. 5 (b) respectively. The proposed model provides an R^2 goodness-of-fit value of 0.891 and 0.899 for the knee and hip respectively. This shows a significant improvement in knee kinematics over the model in [48] with R^2 values of -0.374 and 0.897 for the knee and hip respectively. This improvement is very noticeable in the stance leg kinematics due to the variable stiffness mechanism in the proposed model which can reproduce the weight acceptance phase of walking. Furthermore, it is notable that this similarity is achieved for a model with exact humanlike physical parameters and continuous mass distribution.

The gait displayed by humans is a combination of complex neuromuscular behaviors that would need extremely sophisticated designs to be replicated by a robotic walker. While the humanlike passive walker is unable to provide such accuracy, it is modeled to include the main characteristics of the human gait. One distinctive part in human locomotion is the weight acceptance phase in the stance leg. Unlike other kneed passive walkers with locked stance legs, this behavior is present in the model studied here. If the human knee joint is assumed to act like a torsional spring, the quasi-stiffness of the knee varies in different phases as shown in [53]. Since the value of the knee stiffness is assumed to be constant in the presented model, the instant at which the spring is engaged or disengaged becomes a determining factor in the resulting gait. The ideal instant at which the spring is engaged or disengaged is when the knee angle is equal to the equilibrium angle of the torsional spring. This results in the spring torque imposed on the system to be zero during the transition. It is essential for the spring to become engaged at the equilibrium angle to maintain the passivity of the system since engagement at any other angle would require external energy. In contrast, we have more freedom as to when this spring can be disengaged. While the spring is still preferred to be disengaged at the equilibrium angle, the only negative effect of not doing so would be a slight loss of the energy stored in the stance knee spring. Consequently, we could consider the instant of disengagement as a variable to obtain the desired gait. If the spring remains engaged until the heel-strike, the stance knee passes the equilibrium angle of the spring moments before the impact. Since this angle is slightly above zero, hyperextension in the stance knee is often present in the resulting gait. In contrast, the quasi-stiffness of the human knee drops after the weight acceptance phase which leads to the flexion of the stance knee before the next swing phase. Therefore, in order to adopt this behavior and prevent hyperextension, the torsional spring is preferred to be disengaged as early as possible before the heel-strike. Although this increases the similarity between the gait displayed by the model and humans, obtaining a stable gait becomes considerably more difficult as the energy loss due to the disengagement increases. While an actuator with variable stiffness such as the efficient actuator presented in [54] might be able to simulate the behavior of the human stance knee more accurately, the proposed knee model is preferred as it can maintain the passivity and the simplicity of the design.

Another important aspect of the human gait is the flexion of the swing knee which is necessary for foot clearance. This flexion is slightly smaller in passive models as they lack the required actuation which provides the desired flexion angle. While increasing the slope angle will help with the flexion of the swing knee, it will simultaneously result in higher step lengths. Therefore, a compromise between these parameters is essential to ensure the comparability between the motion of the model and the human gait data.

It is obvious that the presented stable gait in this study is just an example, and the parameters of this model can be altered to obtain other steady gaits on different slopes. However, the overall behavior of the model will remain comparable with humans which allows the parameters to be adapted for different weights and leg lengths without major changes in the gait pattern of the walker.

IV. CONCLUSION

In this paper, we have proposed a 6-link passive walker with flat feet and compliant joints which is modeled to have anthropomorphic physical parameters in addition to the ability to display a very humanlike gait. Unlike previous passive bipeds with knees that were kept locked during the stance phase, the presented model has torsional springs with high stiffness at the knee joints which are engaged at the stance phase and allow the weight acceptance phase of human locomotion to be observable in the gait. The nonlinear equations of the system and the required constraints to obtain the desired gait were derived and the effects of changing the instant of engagement and the disengagement of the knee spring, which substantially affects the resulting gait, were discussed. Despite the sophistication of the model and the limitation of having exact anthropomorphic physical parameters, the initial state vector and the stiffness and damping parameters for a steady gait are obtained and the limit cycles of this gait are studied. Furthermore, the motion of this walker is compared with human gait data in the literature with closely similar weights and step lengths. In comparison with previous attempts at modeling humanlike passive walkers, the presented model with humanlike parameters is drastically more comparable with human gait data.

This work can be extended by exploring the required parameters for steady gaits over different slope angles to represent various step lengths and walking speeds. Moreover, the flat feet in this model can be replaced by a biologically inspired foot to design a more humanlike structure and gait.

Lastly, the suitability of utilizing this model in the process of designing different rehabilitative devices and prosthetic legs can be studied which would allow researchers to simulate these applications with a simple model before conducting time-consuming and costly experiments.

REFERENCES

[1] M. Febrer-Nafría, A. Nasr, M. Ezati, P. Brown, J. M. Font-Llagunes, and J. McPhee, "Predictive multibody dynamic simulation of human neuromusculoskeletal systems: A review," *Multibody Syst. Dyn.*, vol. 58, nos. 3–4, pp. 299–339, Aug. 2023, doi: 10.1007/s11044-022-09852-x.

[2] M. Ezati, B. Ghannadi, and J. McPhee, "A review of simulation methods for human movement dynamics with emphasis on gait," *Multibody Syst. Dyn.*, vol. 47, no. 3, pp. 265–292, Nov. 2019, doi: 10.1007/s11044-019-09685-1.

[3] M. Lamas, F. Mouzo, F. Michaud, U. Lugris, and J. Cuadrado, "Comparison of several muscle modeling alternatives for computationally intensive algorithms in human motion dynamics," *Multibody Syst. Dyn.*, vol. 54, no. 4, pp. 415–442, Apr. 2022, doi: 10.1007/s11044-022-09819-y.

[4] M. A. Paparisabet, R. Dehghani, and A. R. Ahmadi, "Knee and torso kinematics in generation of optimum gait pattern based on human-like motion for a seven-link biped robot," *Multibody Syst. Dyn.*, vol. 47, no. 2, pp. 117–136, Oct. 2019, doi: 10.1007/s11044-019-09679-z.

[5] F. Mouzo, U. Lugris, R. Pamies-Vila, and J. Cuadrado, "Skeletal-level control-based forward dynamic analysis of acquired healthy and assisted gait motion," *Multibody Syst. Dyn.*, vol. 44, no. 1, pp. 1–29, Sep. 2018, doi: 10.1007/s11044-018-09634-4.

[6] M. Febrer-Nafría, R. Pallarès-López, B. J. Fregly, and J. M. Font-Llagunes, "Prediction of three-dimensional crutch walking patterns using a torque-driven model," *Multibody Syst. Dyn.*, vol. 51, no. 1, pp. 1–19, Jan. 2021, doi: 10.1007/s11044-020-09751-z.

[7] Y. Sakagami, R. Watanabe, C. Aoyama, S. Matsunaga, N. Higaki, and K. Fujimura, "The intelligent ASIMO: System overview and integration," in *Proc. IEEE/RSJ Int. Conf. Intell. Robots Syst.*, vol. 3, Sep. 2002, pp. 2478–2483, doi: 10.1109/IRDS.2002.1041641.

[8] S. Collins, A. Ruina, R. Tedrake, and M. Wisse, "Efficient bipedal robots based on passive-dynamic Walkers," *Science*, vol. 307, no. 5712, pp. 1082–1085, Feb. 2005, doi: 10.1126/science.1107799.

[9] T. McGeer, "Passive dynamic walking," *Int. J. Robot. Res.*, vol. 9, no. 2, pp. 62–82, Apr. 1990, doi: 10.1177/027836499000900206.

[10] M. J. Coleman, A. Chatterjee, and A. Ruina, "Motions of a rimless spoked wheel: A simple three-dimensional system with impacts," *Dyn. Stability Syst.*, vol. 12, no. 3, pp. 139–159, Jan. 1997, doi: 10.1080/02681119708806242.

[11] A. D. Kuo, "Energetics of actively powered locomotion using the simplest walking model," *J. Biomechanical Eng.*, vol. 124, no. 1, pp. 113–120, Feb. 2002, doi: 10.1115/1.1427703.

[12] J. Ho Choi and J. W. Grizzle, "Planar bipedal robot with impulsive foot action," in *Proc. 43rd IEEE Conf. Decis. Control (CDC)*, Dec. 2004, pp. 296–302, doi: 10.1109/CDC.2004.1428646.

[13] M. Garcia, A. Chatterjee, A. Ruina, and M. Coleman, "The simplest walking model: Stability, complexity, and scaling," *J. Biomech. Eng.*, vol. 120, no. 2, p. 281, 1998, doi: 10.1115/1.2798313.

[14] A. Goswami, B. Thuilot, and B. Espiau, "Compass-like biped robot—Part I: Stability and bifurcation of passive gaits," Doctoral dissertation, Nat. Inst. Res. Digit. Sci. Technol., France, 1996.

[15] A. Schwab and M. Wisse, "Basin of attraction of the simplest walking model," in *Proc. Int. Design Eng. Tech. Conf. Comput. Inf. Eng.*, vol. 80272, 2001, pp. 531–539, doi: 10.1115/DETC2001/VIB-21363.

[16] A. T. Safa, A. Alasty, and M. Naraghi, "A different switching surface stabilizing an existing unstable periodic gait: An analysis based on perturbation theory," *Nonlinear Dyn.*, vol. 81, no. 4, pp. 2127–2140, Sep. 2015, doi: 10.1007/s11071-015-2130-1.

[17] M. Wisse, D. G. E. Hobbelen, and A. L. Schwab, "Adding an upper body to passive dynamic walking robots by means of a bisecting hip mechanism," *IEEE Trans. Robot.*, vol. 23, no. 1, pp. 112–123, Feb. 2007, doi: 10.1109/TRO.2006.886843.

[18] E. Borzova and Y. Hurmuzlu, "Passively walking five-link robot," *Automatica*, vol. 40, no. 4, pp. 621–629, Apr. 2004, doi: 10.1016/j.automatica.2003.10.015.

[19] T. McGeer, "Passive walking with knees," in *Proc. IEEE Int. Conf. Robot. Autom.*, May 1990, pp. 1640–1645, doi: 10.1109/ROBOT.1990.126245.

[20] M. Wisse, D. Hobbelen, R. Rotteveel, S. Anderson, and G. Zeglin, "Ankle springs instead of arc-shaped feet for passive dynamic Walkers," in *Proc. 6th IEEE-RAS Int. Conf. Humanoid Robots*, Dec. 2006, pp. 110–116.

[21] X. Zang, X. Liu, Y. Liu, S. Iqbal, and J. Zhao, "Influence of the swing ankle angle on walking stability for a passive dynamic walking robot with flat feet," *Adv. Mech. Eng.*, vol. 8, no. 3, Mar. 2016, Art. no. 168781401664201, doi: 10.1177/1687814016642018.

[22] Q. Wang, Y. Huang, and L. Wang, "Passive dynamic walking with flat feet and ankle compliance," *Robotica*, vol. 28, no. 3, pp. 413–425, May 2010, doi: 10.1017/s0263574709005736.

[23] Y. Huang, Q. Wang, B. Chen, G. Xie, and L. Wang, "Modeling and gait selection of passivity-based seven-link bipeds with dynamic series of walking phases," *Robotica*, vol. 30, no. 1, pp. 39–51, Jan. 2012, doi: 10.1017/s0263574711000397.

[24] A. Smyrli and E. Papadopoulos, "Modeling, validation, and design investigation of a passive biped Walker with knees and biomimetic feet," in *Proc. Int. Conf. Robot. Autom. (ICRA)*, May 2022, pp. 193–199, doi: 10.1109/ICRA46639.2022.9812129.

[25] H. Geyer, A. Seyfarth, and R. Blickhan, "Compliant leg behaviour explains basic dynamics of walking and running," *Proc. Roy. Soc. B, Biol. Sci.*, vol. 273, no. 1603, pp. 2861–2867, Nov. 2006, doi: 10.1098/rspb.2006.3637.

[26] J. Adolfsson, H. Dankowicz, and A. Nordmark, "3D passive Walkers: Finding periodic gaits in the presence of discontinuities," *Nonlinear Dyn.*, vol. 24, no. 2, pp. 205–229, 2001, doi: 10.1023/A:1008300821973.

[27] M. R. Sabaapour, M. R. Hairi Yazdi, and B. Beigzadeh, "Passive turning motion of 3D rimless wheel: Novel periodic gaits for bipedal curved walking," *Adv. Robot.*, vol. 29, no. 5, pp. 375–384, Mar. 2015, doi: 10.1080/01691864.2014.1001788.

[28] M. R. Sabaapour, M. R. Hairi Yazdi, and B. Beigzadeh, "Passive dynamic turning in 3D biped locomotion: An extension to passive dynamic walking," *Adv. Robot.*, vol. 30, no. 3, pp. 218–231, Feb. 2016, doi: 10.1080/01691864.2015.1107500.

[29] M. Wisse and J. V. Frankenhuyzen, "Design and construction of mike; A 2-D autonomous biped based on passive dynamic walking," in *Adaptive Motion of Animals and Machines*. Berlin, Germany: Springer, 2006, pp. 143–154.

[30] S. H. Collins, M. Wisse, and A. Ruina, "A three-dimensional passive-dynamic walking robot with two legs and knees," *Int. J. Robot. Res.*, vol. 20, no. 7, pp. 607–615, Jul. 2001, doi: 10.1177/02783640122067561.

[31] K. Wang, P. T. Tobajas, J. Liu, T. Geng, Z. Qian, and L. Ren, "Towards a 3D passive dynamic Walker to study ankle and toe functions during walking motion," *Robot. Auto. Syst.*, vol. 115, pp. 49–60, May 2019, doi: 10.1016/j.robot.2019.02.010.

[32] M. Wisse, A. L. Schwab, R. Q. van der Linde, and F. C. T. van der Helm, "How to keep from falling forward: Elementary swing leg action for passive dynamic Walkers," *IEEE Trans. Robot.*, vol. 21, no. 3, pp. 393–401, Jun. 2005, doi: 10.1109/TRO.2004.838030.

[33] B. Beigzadeh, M. R. Sabaapour, M. R. H. Yazdi, and K. Raahemifar, "From a 3D passive biped Walker to a 3D passivity-based controlled robot," *Int. J. Humanoid Robot.*, vol. 15, no. 4, Aug. 2018, Art. no. 1850009, doi: 10.1142/s0219843618500093.

[34] H. Gritli, S. Belghith, and N. Khraief, "OGY-based control of chaos in semi-passive dynamic walking of a torso-driven biped robot," *Nonlinear Dyn.*, vol. 79, no. 2, pp. 1363–1384, Jan. 2015, doi: 10.1007/s11071-014-1747-9.

[35] H. Gritli and S. Belghith, "Bifurcations and chaos in the semi-passive bipedal dynamic walking model under a modified OGY-based control approach," *Nonlinear Dyn.*, vol. 83, no. 4, pp. 1955–1973, Mar. 2016, doi: 10.1007/s11071-015-2458-6.

[36] T. Kobayashi, T. Aoyama, Y. Hasegawa, K. Sekiyama, and T. Fukuda, "Adaptive speed controller using swing leg motion for 3-D limit-cycle-based bipedal gait," *Nonlinear Dyn.*, vol. 84, no. 4, pp. 2285–2304, Jun. 2016, doi: 10.1007/s11071-016-2645-0.

[37] B. Beigzadeh, A. Meghdari, and S. Sohrabpour, "Passive dynamic object manipulation: Preliminary definition and examples," *Acta Automatica Sinica*, vol. 36, no. 12, pp. 1711–1719, Dec. 2010, doi: 10.1016/s1874-1029(09)60067-7.

[38] B. Beigzadeh, A. Meghdari, and S. Sohrabpour, "Passive dynamic object manipulation: A framework for passive walking systems," *Proc. Inst. Mech. Eng., K, J. Multi-body Dyn.*, vol. 227, no. 2, pp. 185–198, Jun. 2013, doi: 10.1177/1464419313478525.

[39] H. Geyer and H. Herr, "A muscle-reflex model that encodes principles of legged mechanics produces human walking dynamics and muscle activities," *IEEE Trans. Neural Syst. Rehabil. Eng.*, vol. 18, no. 3, pp. 263–273, Jun. 2010, doi: 10.1109/TNSRE.2010.2047592.
[40] C. Honeycutt, J. Sushko, and K. B. Reed, "Asymmetric passive dynamic Walker," in *Proc. IEEE Int. Conf. Rehabil. Robot.*, Jun. 2011, pp. 1–6, doi: 10.1109/ICORR.2011.5975465.
[41] J. Sushko, C. Honeycutt, and K. B. Reed, "Prosthesis design based on an asymmetric passive dynamic Walker," in *Proc. 4th IEEE RAS EMBS Int. Conf. Biomed. Robot. Biomechatronics (BioRob)*, Jun. 2012, pp. 1116–1121, doi: 10.1109/BIOROB.2012.6290293.
[42] B. Beigzadeh and S. A. Razavi, "Dynamic walking analysis of an underactuated biped robot with asymmetric structure," *Int. J. Humanoid Robot.*, vol. 18, no. 4, Aug. 2021, Art. no. 2150014, doi: 10.1142/s0219843621500146.
[43] M. J. Miandoab and B. Beigzadeh, "Asymmetric three-link passive Walker," *Nonlinear Dyn.*, vol. 111, no. 10, pp. 9145–9159, May 2023, doi: 10.1007/s11071-023-08316-x.
[44] Y. Aoustin and A. M. Formalskii, "Walking of biped with passive exoskeleton: Evaluation of energy consumption," *Multibody Syst. Dyn.*, vol. 43, no. 1, pp. 71–96, May 2018, doi: 10.1007/s11044-017-9602-7.
[45] S. M. Moghadam, M. S. Talarposhti, A. Niaty, F. Towhidkhah, and S. Jafari, "The simple chaotic model of passive dynamic walking," *Nonlinear Dyn.*, vol. 93, no. 3, pp. 1183–1199, Aug. 2018, doi: 10.1007/s11071-018-4252-8.
[46] S. L. Delp, F. C. Anderson, A. S. Arnold, P. Loan, A. Habib, C. T. John, E. Guendelman, and D. G. Thelen, "OpenSim: Open-source software to create and analyze dynamic simulations of movement," *IEEE Trans. Biomed. Eng.*, vol. 54, no. 11, pp. 1940–1950, Nov. 2007, doi: 10.1109/TBME.2007.901024.
[47] S. Apte, M. Plooij, and H. Vallery, "Simulation of human gait with body weight support: Benchmarking models and unloading strategies," *J. NeuroEng. Rehabil.*, vol. 17, no. 1, pp. 1–16, Dec. 2020, doi: 10.1186/s12984-020-00697-z.
[48] I. Handžic and K. B. Reed, "Validation of a passive dynamic Walker model for human gait analysis," in *Proc. 35th Annu. Int. Conf. IEEE Eng. Med. Biol. Soc. (EMBC)*, Jul. 2013, pp. 6945–6948.
[49] R. Dumas and J. Wojtusch, "Estimation of the body segment inertial parameters for the rigid body biomechanical models used in motion analysis," in *Handbook of Human Motion*. Cham, Switzerland: Springer, 2017, pp. 1–31.
[50] E. R. Westervelt, J. W. Grizzle, C. Chevallereau, J. H. Choi, and B. Morris, *Feedback Control of Dynamic Bipedal Robot Locomotion*. Boca Raton, FL, USA: CRC Press, 2018.
[51] J. R. Dormand and P. J. Prince, "A family of embedded Runge-Kutta formulae," *J. Comput. Appl. Math.*, vol. 6, no. 1, pp. 19–26, Mar. 1980.
[52] C. Schreiber and F. Moissenet, "A multimodal dataset of human gait at different walking speeds established on injury-free adult participants," *Sci. Data*, vol. 6, no. 1, pp. 1–7, Jul. 2019, doi: 10.1038/s41597-019-0124-4.
[53] K. Shamaei, G. S. Sawicki, and A. M. Dollar, "Estimation of quasi-stiffness of the human knee in the stance phase of walking," *PLoS ONE*, vol. 8, no. 3, Mar. 2013, Art. no. e59993, doi: 10.1371/journal.pone.0059993.
[54] L. C. Visser, R. Carloni, and S. Stramigioli, "Energy-efficient variable stiffness actuators," *IEEE Trans. Robot.*, vol. 27, no. 5, pp. 865–875, Oct. 2011, doi: 10.1109/TRO.2011.2150430.

MAHAN JABERI MIANDOAB received the B.Sc. degree in mechanical engineering and the M.Sc. degree in biomedical engineering from Iran University of Science and Technology, Tehran, Iran, in 2019 and 2022, respectively. He is currently pursuing the Ph.D. degree in mechanical engineering with the University of Calgary, Calgary, Canada.

He was a member of the Biomechatronics and Cognitive Engineering Research Laboratory, Iran University of Science and Technology, from 2019 to 2022, before joining the Adaptive Bionics Laboratory, University of Calgary, in 2023.

MOHAMMAD REZA HAGHJOO received the M.Sc. degree in mechanical engineering from the Sharif University of Technology, Tehran, Iran, in 2007, and the Ph.D. degree in mechanical engineering from the University of Tehran, Tehran, in 2015.

From 2016 to 2017, he was a Postdoctoral Researcher with the Robots and Intelligent Systems Laboratory, Gyeongsang National University, Jinju, South Korea, and with the Intelligent Medical Robotics Laboratory, Gwangju Institute of Science and Technology, Gwangju, South Korea, respectively. In 2019, he joined the Faculty of Mechanical and Energy Engineering, Shahid Beheshti University, Tehran, where he is currently an Assistant Professor. His current research interests include legged robots, rehabilitation, and servo mechanisms.

BORHAN BEIGZADEH received the B.Sc. degree in mechanical engineering from the University of Tehran, in 2003, and the M.Sc. and Ph.D. degrees in mechanical engineering from the Sharif University of Technology, in 2005 and 2011, respectively. Then, he joined Iran University of Science and Technology, Tehran, Iran, where he is currently an Associate Professor with the School of Mechanical Engineering and established the Biomechatronics and Cognitive Engineering Research Laboratory. His current research interests include non-linear dynamics and control, robotics, biomechatronics, and cognitive engineering.